EMBRY-RIDDLE
Aeronautical University™
SCHOLARLY COMMONS

Publications

Mechanisms of Field-Aligned Current Formation in Magnetic Reconnection

Xuanye Ma
University of Alaska, Fairbanks, max@erau.edu

Antonius Otto
University of Alaska, Fairbanks

Follow this and additional works at: https://commons.erau.edu/publication

Part of the Astrophysics and Astronomy Commons

Scholarly Commons Citation

Ma, X., & Otto, A. (2013). Mechanisms of Field-Aligned Current Formation in Magnetic Reconnection. *Journal of Geophysical Research: Space Physics, 118*(8). https://doi.org/10.1002/jgra.50457

Mechanisms of field-aligned current formation in magnetic reconnection

Xuanye Ma[1] and Antonius Otto[1]

[1]   Satellite observations provide strong evidence for the generation of significant field-aligned currents (FACs) during magnetic reconnection. Reconnection of antiparallel magnetic field does not generate FACs in magnetohydrodynamics (MHD) due to coplanarity in MHD shocks. However, a guide magnetic field and a sheared velocity component are almost always present at the magnetopause and their absence is a singular case. It is illustrated that the presence of these noncoplanar fields requires FACs. Contrary to intuition, such currents are generated more efficiently for a small guide field and are more likely to be a result of the redistribution of already present FACs for large guide fields. It is demonstrated that moderate values of shear flow can generate significant ionospheric FACs. Similar to shear flow, the presence of Hall physics leads to significant FACs and we examine the scaling of these current with the ion inertia length.

1. Introduction

[2] Field-aligned current (FAC), the component of the electric current in the magnetic field direction, plays an important role for the solar wind-magnetosphere-ionosphere coupling and the generation of high energy particles [*Sato and Iijima*, 1979; *Wang et al.*, 2001]. However, the generation of FACs is not trivial. For example, in single particle theory, all of the first-order drift velocities, and thereby drift currents, are perpendicular to the magnetic field. Without an evolution equation for FACs, the generation of FACs has not been fully understood.

[3] It is often suggested to divide the divergence of the FAC into pressure gradient term and inertia term by applying the momentum equation [*Vasyliunas*, 1984]. However, this method represents force balance, which does not provide a causal source of FACs. According to the definition of evolution of FAC, we have

$$\frac{\partial j_\parallel}{\partial t} = \hat{\mathbf{b}} \cdot \frac{\partial \mathbf{j}}{\partial t} + \mathbf{j} \cdot \frac{\partial \hat{\mathbf{b}}}{\partial t}, \qquad (1)$$

which implies that the generation of FACs requires either current bent into magnetic field direction or vice versa. By taking the curl of the induction equation, one can get approximately

$$\frac{\partial j_\parallel}{\partial t} = \nabla_\parallel (\mathbf{B} \cdot \mathbf{\Omega}) - \nabla_\parallel (\mathbf{V} \cdot \mathbf{j}) + \nabla^2 (\eta j_\parallel), \qquad (2)$$

[1]Geophysical Institute, University of Alaska Fairbanks, Fairbanks, Alaska, USA.

Corresponding author: X. Ma, Geophysical Institute, University of Alaska Fairbanks, 903 Koyukuk Drive, Fairbanks, AK 99775-7320, USA. (xma2@alaska.edu)

with an inner product of $\hat{\mathbf{b}} = \mathbf{B}/B$ from the left-hand side and where $\nabla_\parallel = \hat{\mathbf{b}} \cdot \nabla$, $j_\parallel = \hat{\mathbf{b}} \cdot \mathbf{j}$, $\mathbf{\Omega} = \nabla \times \mathbf{V}$, and B is the field magnitude [*Ogino*, 1986]. Here all quantities are normalized by typical values, which will be discussed in section 2. The first term on the right-hand side of equation (2) is the field-aligned vorticity term. A physical process associated with this term is the generation of helical magnetic field by twisting the field lines and thereby generating FAC. The second term on the right-hand side of equation (2) represents the shear flow along the current direction. A physical process associated with this term is bending of the magnetic field lines into the current direction. The last term on the right-hand side of equation (2) indicates the dissipation of FAC by the resistivity, which is an approximation of $\hat{\mathbf{b}} \cdot \nabla^2 \mathbf{j}$ and is important in the ionosphere. Note the term $\mathbf{j} \cdot \partial_t \hat{\mathbf{b}}$ in equation (1), which is ignored in equation (2), can also be important for FAC. In reality, these physical processes may operate simultaneously. However, a strict FAC evolution equation from the induction equation appears too complicated to reveal useful physical insight.

[4] From the perspective of magnetohydrodynamics (MHD) waves, it is suggested that FACs are generated and carried by the Alfvén wave [*Cao and Kan*, 1987; *Song and Lysak*, 1994]. Other authors focused on the specific conditions, i.e., FAC generation in three-dimensional reconnection configuration [*Sato et al.*, 1983, 1984; *Ogino*, 1986; *Birn*, 1989; *Birn and Hesse*, 1991; *Scholer and Otto*, 1991; *Ugai*, 1991; *Ma et al.*, 1995; *Ma and Lee*, 1999, 2001]. Both region 1 and region 2 FACs can be obtained by triggering reconnection in the taillike configuration [*Scholer and Otto*, 1991]. In a local three-dimensional reconnection configurations, it has been demonstrated that FACs are generated because the magnetic field lines are bent toward the main current direction by shear flow and pressure gradients [*Ma et al.*, 1995; *Ma and Lee*, 1999].
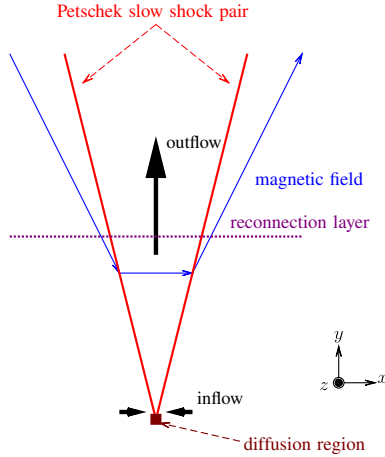
Figure 1. Sketch of Petschek reconnection.

[5] Although the generation of FAC in reconnection is considered an important three-dimensional feature, FAC generation has also been reported in two-dimensional reconnection [*Lin*, 2001]. In two dimensions, the transition of the plasma properties (density, velocity, pressure, and magnetic field) from one inflow region through the outflow region to the other inflow region is mostly one dimensional and is achieved in general through a series of MHD waves and discontinuities. Such a layer structure is called "reconnection layer". In two-dimensional reconnection, it is a cut across the steady state inflow and outflow regions, see Figure 1. In this paper, we focus on the generation of FAC in two-dimensional reconnection. Two-dimensional simulations are supplemented by one-dimensional studies of the associated Riemann problem [*Lin and Lee*, 1993] of the reconnection layer. In situ satellite observation indicated that reconnection layer structure still exists in the approximately steady state regions of three-dimensional reconnection [*Walthour et al.*, 1995].

[6] In the traditional Petschek reconnection model, the inflow and outflow regions are divided by a pair of switch-off shocks (see Figure 1) [*Petschek*, 1964]. Due to coplanarity in MHD shocks, there is no FAC in Petschek reconnection. However, Petschek's model is a singular case in the real physical world, and a finite guide field component is always present [e.g., *Lee et al.*, 2002]. At the dayside magnetopause and away from the subsolar point, there is also always a substantial shear flow perpendicular to the antiparallel magnetic field components, due to the magnetosheath flow. Hereafter, we refer to the plane in which reconnection operates as the reconnection plane. Coplanarity implies that the magnetic field components tangential to a discontinuity are parallel or antiparallel (the magnetic field vectors are in a single plane). This renders the current always perpendicular to the magnetic field, and a field-aligned current requires noncoplanar magnetic fields, e.g., a guide field perpendicular to the reconnection plane. A shear plasma flow component perpendicular to the reconnection plane is referred as "perpendicular shear flow". For example, in Figure 1, the xy plane is the reconnection plane and the magnetic field and bulk velocity z component is the noncoplanar field. In a reconnection configuration involving a noncoplanar field (caused by a guide field component or a perpendicular shear flow), the pair of switch-off shocks in Petschek reconnection is replaced by a pair of slow shocks and a pair of rotational discontinuities (RDs) in ideal MHD (not shown in Figure 1) [*Lin and Lee*, 1993; *Sun et al.*, 2005]. In resistive MHD, the RD becomes the time-dependent intermediate shock (TDIS) [*Lin et al.*, 1992]. Strictly, the width of the RD is zero and the FAC in the RD is a delta function, because there is no intrinsic scale in ideal MHD. Therefore, a physical FAC can only be generated by the TDIS, while the slow shocks do not generate FACs, due to coplanarity. However, in the sense that resistive effects are negligible, i.e., the total tangential magnetic field remains constant through the TDIS, we still use RD to refer to this transition layer. In this paper, we use TDIS to emphasize a finite width of this transition layer.

[7] The influence of Hall physics on the generation of the FAC is important and is also investigated in this study, because the typical length scale of the diffusion region in the onset of reconnection is on the ion or even on the electron inertia scale. The inclusion of the Hall term in the induction equation leads to the separation of the ion and electron velocity, and the frozen-in condition only applies to the electrons, which move antiparallel to the current in a thin current sheet. This electron motion strongly modifies the reconnection layer and causes the B_z bipolar signature. Therefore, the effect of Hall physics is similar to the effect of shear flow in ordinary MHD.

[8] In this study, we focus on the above three selected cases, i.e., (1) reconnection with a guide magnetic field component, (2) reconnection with a perpendicular shear flow, and (3) Hall MHD reconnection. The reconnection layer structures are examined by using both one- and two-dimensional simulations. The dependence of the FAC generation on the magnitude of guide field component, shear flow, and Hall parameter is systematically investigated by one-dimensional simulation confirmed by two-dimensional simulations of selected cases.

2. Numerical Model

2.1. Physical Quantity Associated With FAC

[9] Several physical quantities associated with the FAC's are considered to characterize the generation of FAC. The profile of the FAC density $j_\parallel$ provides detailed information of the FAC distribution. In order to compare FAC generation for varying parameters, the FAC density magnitude max $|j_\parallel|$ is used to represent the each specific case. Both convection (or redistribution) and generation of the FAC can change the local FAC density. As we have demonstrated in section 1, the complete FACs' evolution equation is rather complicated and we doubt that an interpretation in physical terms is possible or unique. Therefore, we apply a much simpler concept, i.e., ask the question whether the integral field-aligned current in one direction changes in the case of reconnection when compared to the initial current sheet equilibrium. If the integral current is approximately constant, we use the term "redistribution". In one-dimensional configurations, the integral of the FAC density $I_\parallel = \int |j_\parallel| \mathrm{d}x$ is the surface current. Since the magnetic field is a solenoidal field, the magnetic flux $\Phi = Bs$ is a constant value along the magnetic field, where s is the cross sectional area of a magnetic field flux tube. Therefore, $i_\parallel = j_\parallel/B$ represents FAC in this study. By using the same argument ($\nabla \cdot \mathbf{j} = 0$), the FAC quantity $i_\parallel$
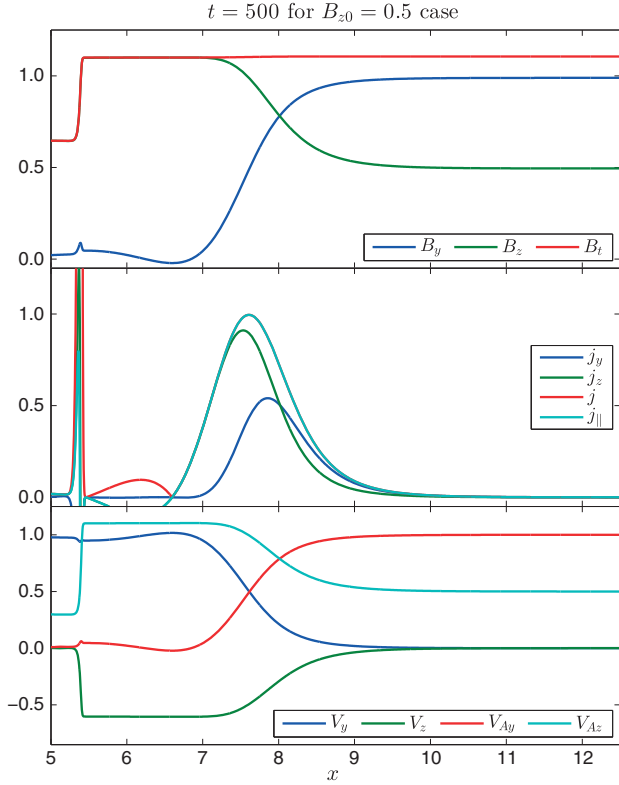
Figure 2. Profile of the reconnection layer at $t = 500$ for $B_{z0} = 0.5$ and $p_\infty = 0.25$ case. The top panel shows B_y, B_z, and B_t, the middle panel shows j_y, j_z, j, and $j_\|$, and the bottom panel shows V_y, V_z, V_{Ay}, and V_{Az}.

should remain constant along the flux tube in the absence of perpendicular currents. Thus, for mapping from magnetosphere into the ionosphere, the total FAC which is supposed to be conserved, is more important than max $|j_\||$. Therefore, we include the integral $K_\| = \int |i_\||dx$ in the following investigation.

2.2. Numerical Algorithm

[10] The full set of the resistive Hall MHD equations and its numerical solver has been discussed by *Otto* [1990, 2001]. In the computations, all quantities are normalized to the typical values, that is, the length scales L to a typical length L_0, the density ρ to $\rho_0 = n_0 m_0$ with the number density n_0 and the ion mass m_0, the magnetic field **B** to B_0, the velocity **V** to the typical Alfvén velocity $V_A = B_0(\mu_0\rho_0)^{-1/2}$, the thermal pressure p to $P_0 = B_0^2/(2\mu_0)$, and the time t to a typical Alfvén transit time $T_A = L_0/V_A$. The Hall parameter $l = \lambda_i/L_0$ is the ratio of ion inertia length λ_i to the typical length scale L_0. The basic Petschek reconnection is sketched in Figure 1, and the one- and two-dimensional simulations use the same coordinate system. The initial equilibrium is a one-dimensional modified Harris sheet, which is given by **B** $= [0, \tanh(x), B_{z0}]$, **V** $= [0, 0, V_{z0} \tanh(x)]$, $p = p_\infty + 1 - B_y^2$, and $\rho = 1$, where $p_\infty = 0.25$ is the inflow thermal pressure. Here the values of B_{z0} and V_{z0} represent the magnitude of the guide field and shear flow, respectively, and are discussed in each case study.

[11] The two-dimensional reconnection simulations are performed in a rectangular box with $|x| \le 30$ and $0 \le y \le$

120, which is resolved by using 203×403 grid points with a nonuniform grid along the x and y directions. To sufficiently resolve the diffusion region, the best resolution is set to 0.1 and 0.2 in the x and y directions in the diffusion region. Free boundary conditions ($\partial_n = 0$, where ∂_n represents the partial derivative in the direction normal to the boundary) are applied to the x maximum and minimum boundary and y maximum boundary. The y minimum boundary is determined by symmetry properties of the (Hall) MHD equations [*Otto et al.*, 2007]. In the simulation, we use the following resistivity model

$$\eta = \eta_0 \left[1 - \exp(-t/t_0)\right]/\left[\cosh(x)\cosh(y)\right] + \eta_b, \quad (3)$$

where $\eta_0 = 0.05$, $t_0 = 3$, and $\eta_b = 0.002$ is the background resistivity to smooth the numerical dispersion. The first term is a resistivity used to determine the location and size of the diffusion region, and it is gradually switched on to trigger magnetic reconnection.

[12] One-dimensional simulations of the Riemann problem are used to better resolve the physics in the reconnection layer, which has the advantage to allow much higher resolution with shorter execution times and better accuracy (uniform grid with $\Delta x = 0.004$ and 0.01 for MHD and Hall MHD cases, respectively). The reconnection layer can be initialized by adding a small constant B_n ($= B_x = 0.025$ in this study) component to our one-dimensional initial equilibrium [*Lin and Lee*, 1993, 1999]. A very small resistivity η of 2×10^{-4} is included for all cases.

3. Simulation Results

3.1. Guide Field Cases

[13] The Harris sheet has a current in the z direction. Therefore, the presence of a magnetic guide field B_z component implies the presence of a FAC in the initial configuration, which is simply a projection effect. However, it is not clear whether there is additional FAC generated in the reconnection process or if the preexisting FACs are just redistributed. Figure 2 shows the profile of the reconnection layer at $t = 500$ for $B_{z0} = 0.5$, $V_{z0} = 0$ case. The top panel shows the antiparallel magnetic component, B_y, guide field component, B_z, and tangential magnetic field component, $B_t = \sqrt{B_y^2 + B_z^2}$, the middle panel shows the current density j_y, j_z component, total current density j, and FAC density $j_\|$, and the bottom panel shows the velocity V_y, V_z component, Alfvén velocity $V_{Ay} = B_y/\sqrt{\rho}$, and $V_{Az} = B_z/\sqrt{\rho}$ component.

[14] From the inflow to the outflow region, the tangential magnetic field B_t is constant through the TDIS, while the B_y component decreases to zero, and the B_z component increases to the value of magnetic B_t component. The middle panel shows that the FAC density $j_\|$ (light blue) is almost identical to the total current j (red) in the TDIS, due to the tiny normal magnetic field component. The total current density is actually masked by the FAC density. The RD layer is basically a force-free field added to a constant normal field, and it is consistent with the constant tangential magnetic field. Thus, the pressure gradient term in the equation introduced by *Vasyliunas* [1984] is zero. The bottom panel shows that the change of the tangential velocity follows the Walén relation. The small bump of magnetic B_y component in the slow shock is likely a numerical error, which leads an
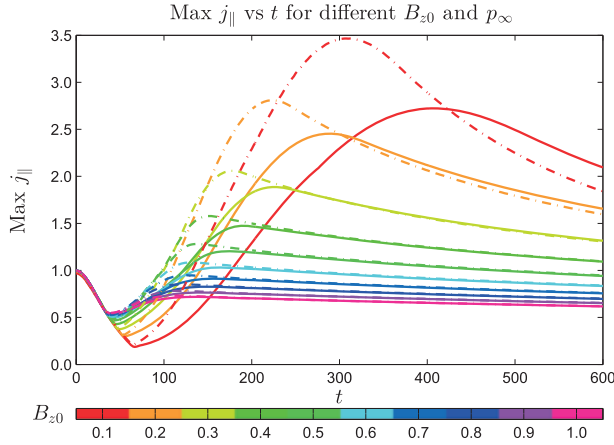
Figure 3. The evolution of $\max j_\parallel$ in the reconnection layer for different B_{z0} and p_∞ cases. The color index indicates B_{z0} varying from 0.1 to 1; the dashed and solid lines represent the $p_\infty = 0.25$ and 0.5 cases, respectively.

artificial FAC in the slow shock layer. The integral of this FAC is small. This configuration is in contrast to Petschek reconnection, which is the no-guide field case. In the Petschek reconnection layer, there is no B_z component and B_y component is vanished by the switch-off shock from inflow region to outflow region. Therefore, there is no FAC in Petschek reconnection.

[15] Figure 3 depicts the evolution of the maximum FAC density in the reconnection layer for different B_{z0} and p_∞ cases. Note due to the symmetry, the FAC density are always positive in this configuration. The color index represents the value of B_{z0} ranging from 0.1 to 1; the dashed and solid lines represent the $p_\infty = 0.25$ and 0.5 cases, respectively. At $t = 0$, $\max j_\parallel = j_\parallel(x = 0) = 1$ for all cases. For Harris sheet, the maximum current density $j_z = 1$ is in the center of the current sheet, where magnetic field and FAC density are zero. Therefore, an arbitrarily small positive B_{z0} implies a FAC density $j_\parallel$ of 1 and an arbitrarily small negative B_{z0} implies a FAC density $j_\parallel = -1$. This indicates a singularity of the Harris sheet for FAC density, although the integral of the FAC converges to zero in the limit of antiparallel magnetic fields. The period of decreasing $\max j_\parallel$ ($t < 100$ in Figure 3) is the relaxation time for generating the slow shocks and intermediate shocks, which appears longer for a smaller guide field case. Theoretically, a simple RD should be independent of upstream thermal pressure p_∞. However, Figure 3 shows that smaller p_∞ cases have higher $\max j_\parallel$ peaks in the reconnection layer, which indicates that the peak of $\max j_\parallel$ is influenced by the slow shock. The dashed and solid lines eventually tend to converge, which is an indication of the separation of the RD and the slow shock. The asymptotic state of the RD is insensitive to the inflow thermal pressure or plasma beta. Figure 3 also demonstrates that smaller guide field generates higher $\max j_\parallel$, because the rotation of the tangential magnetic field through the TDIS is less for a larger guide field. If the reference magnetic field (normalization) is based on the total magnetic field, a large guide field component implies a small value of the antiparallel magnetic field components, such that magnetic reconnection is expected to be slower. We note that large plasma beta β in the presence

of a guide field and strong magnetic field asymmetry can stabilize magnetic reconnection [*Swisdak et al.*, 2003].

[16] Figure 4 shows the evolution of the surface current $I_\parallel$ for different guide field magnitudes B_{z0} ($p_\infty = 0.25$ for those cases). It shows that $I_\parallel$ is initially proportional to the guide field magnitude B_{z0} and converges to values between 2.2 and 2.5, which is a rather small range compared to the variation of the initial values. This indicates that the overall evolving FAC is not very sensitive to the magnetic guide field value. FACs are generated more efficiently for a small B_{z0} case and are more likely redistributed for a large B_{z0} case. However, convergence to the asymptotic state takes longer for small B_z values.

[17] Figure 5 shows the evolution of $K_\parallel$ for different guide field magnitudes B_{z0} ($p_\infty = 0.25$ for those cases), which demonstrates that $K_\parallel$ is nearly independent of time. This is because FACs propagate with the rotational discontinuity, and the dissipation is very small in our system. Note $K_\parallel$ decreases with increasing B_{z0} which seems inconsistent with the limit of $B_z = 0$ where $K_\parallel = 0$. This limit is indeed not analytic due to the singularity of the $j_\parallel$ in the Harris sheet. However, $I_\parallel$ is analytic because the integral current converges to 0 and the current is nonzero only in an arbitrarily small vicinity of $x = 0$. It is noted that the issue of FAC in the limit of B_z to 0 is somewhat questionable in MHD because of an extreme concentration of the FAC. This is also supported by and consistent with the very slow evolution to an asymptotic state for very small B_z.

[18] In conclusion, our simulations demonstrate that reconnection with a small guide field can generate more FAC; however, it takes larger temporal and spatial scale to achieve its asymptotic state. Note that our one-dimensional simulations cover a much longer period than the two-dimensional simulations. The normal magnetic field $B_n = 0.025$ in our one-dimensional simulations yields to a reconnection rate $E_r = B_n V_A = 0.025$, which is about 4 times slower than the typical two-dimensional Petschek reconnection rate (~ 0.1). Thus, to compare with two-dimensional evolution and length scales, we would increase the normal magnetic field by a factor of 4, which implies a 4 times faster evolution of the waves. As a result, it takes about $150 T_A$ to achieve the asymptotic status for small guide field case in two-dimensional reconnection. For comparison with the real
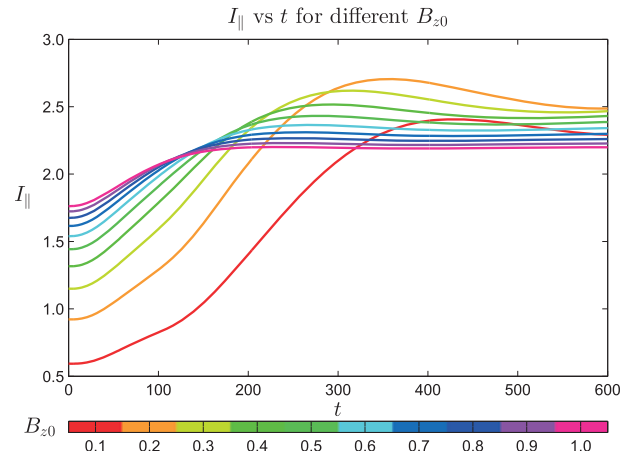

Figure 4. The evolution of $I_\parallel$ in the reconnection layer for different B_{z0} and $p_\infty = 0.25$ cases.
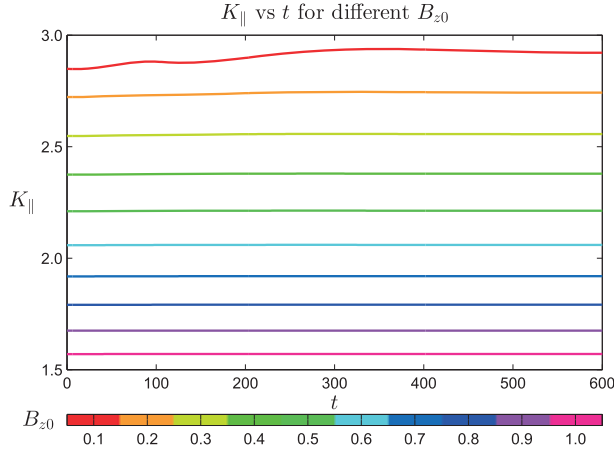
Figure 5. The evolution of $K_\parallel$ in the reconnection layer for different B_{z0} and $p_\infty = 0.25$ cases.

magnetopause, we assume that the typical magnetic field is 20 nT, density is $0.1 \sim 10$ cm^{-3}. Since the diffusion region is likely on the ion inertia scale, which is also the limitation of MHD, we use ion inertia length as the typical length scale, which is about 400 km at the magnetopause. Based on these parameters, for a small guide field ($B_z = 0.1$) case, reconnections takes about 1 to 7 min to reach its asymptotic state, which seems likely relevant to the observation.

3.2. Shear Flow Cases

[19] For shear flow along the z direction, the frozen-in condition implies a drag of reconnected magnetic field lines into opposite directions on the two sides of the outflow region, which generates a B_z component. Figure 6 shows the magnetic field B_z component (isosurface) and the FAC density $j_\parallel$ indicated by color at $t = 180$ for a perpendicular shear flow case ($B_{z0} = 0$ and $V_{z0} = 0.5$). It illustrates that a large B_z component occurs in combination with a strong FAC. We find all of the FACs are on reconnected field lines. It has been demonstrated that the reconnection layer is also composed of a pair of slow shocks and a pair of RDs for this configuration, which is similar to the guide field case [*Sun et al.*, 2005].
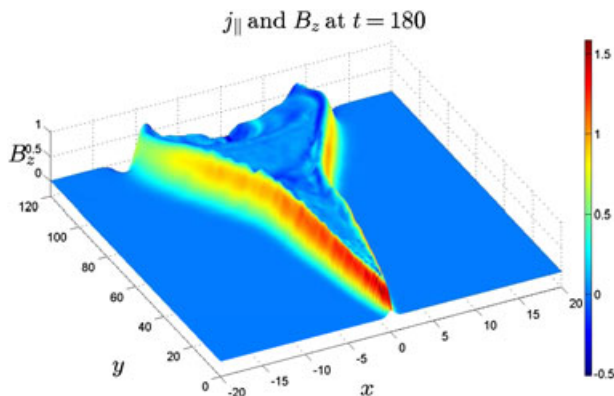

Figure 6. FAC density $j_\parallel$ (color) and magnetic field B_z component (isosurface) at $t = 180$ for magnetic reconnection with perpendicular shear flow case.
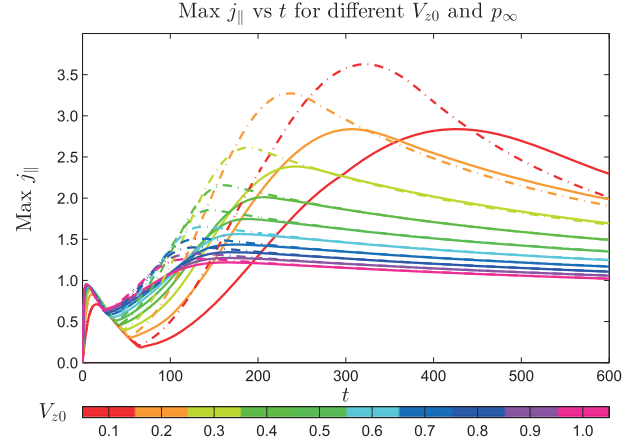

Figure 7. The evolution of max $j_\parallel$ in the reconnection layer for different V_{z0} and p_∞ cases. The color index indicates V_{z0} varying from 0.1 to 1; the dashed and solid lines represent for $p_\infty = 0.25$ and 0.5 cases, respectively.

[20] Figure 7 shows the evolution of max $j_\parallel$ in the reconnection layer for different V_{z0} and p_∞ cases, which is rather similar to Figure 3, except that the initial FAC is zero in this configuration. Similar to the guide field cases, max $j_\parallel$ decreases with increasing of shear flow and a very small shear flow magnitude requires a long time to relax to the asymptotic state. Note that despite the same magnetic field rotation angle (90°) for all the case, a large shear flow has a wider transition layer, which may be the consequence of the constraint of the Walén relation and energy conservation. And the straightforward physical reason for this behavior is not clear yet. It is also noted that the asymptotic value of the maximum FAC density is higher in the shear flow cases when compared to the guide field presence.

[21] Figure 8 shows the evolution of surface FAC $I_\parallel$ in the reconnection layer for different V_{z0} ($p_\infty = 0.25$ in these cases), which is similar to Figure 4. At an early stage, $I_\parallel$ increases with increasing V_{z0} initially and most curves appears to converge toward an asymptotic value of about 3.0 at the later times. The surface FAC also measures the magnetic field rotation around the main direction (x direction), which is 90° for all cases. Therefore, the surface FAC is not
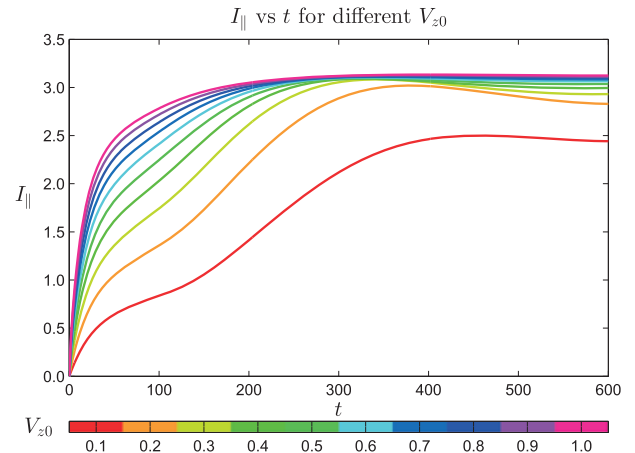

Figure 8. The evolution of $I_\parallel$ in the reconnection layer for different V_{z0} and $p_\infty = 0.25$ cases.
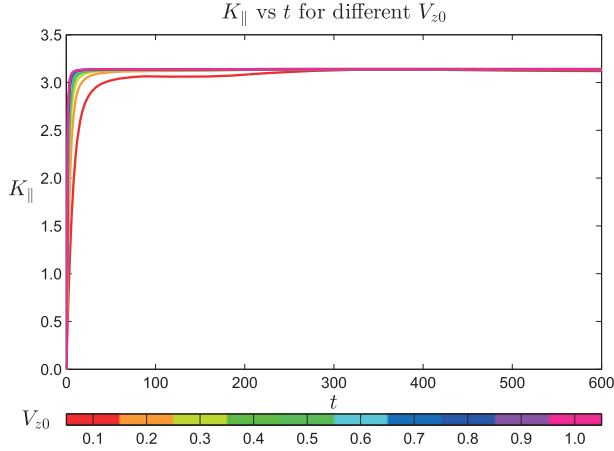
Figure 9. The evolution of $K_\parallel$ in the reconnection layer for different V_{z0} and $p_\infty = 0.25$ cases.

sensitive to the value of V_{z0}. For the small shear flow cases ($V_{z0} \leq 0.2$ cases), it takes more time to achieve relativity lower asymptotic value, which indicates that there may exist a low critical value for shear flow to generate significative amount of FAC.

[22] The evolution of total FAC $K_\parallel$ for different shear flow magnitudes V_{z0} ($p_\infty = 0.25$ for those cases) is presented in Figure 9, which shows an even stronger tendency to converge to a fixed value of close to 3.2 for all cases. Also, the rise time is much shorter. Therefore, even moderate values of shear flow should generate significant ionospheric FACs. Note the rise time is consistent with the relaxation time for generating the slow and intermediate shocks, see Figure 7, which implies that FACs are generated by the formation of RDs. There is no rise time for guide field configuration, since most of the current is already in the magnetic field direction. In general, it appears that shear flow generates a larger value
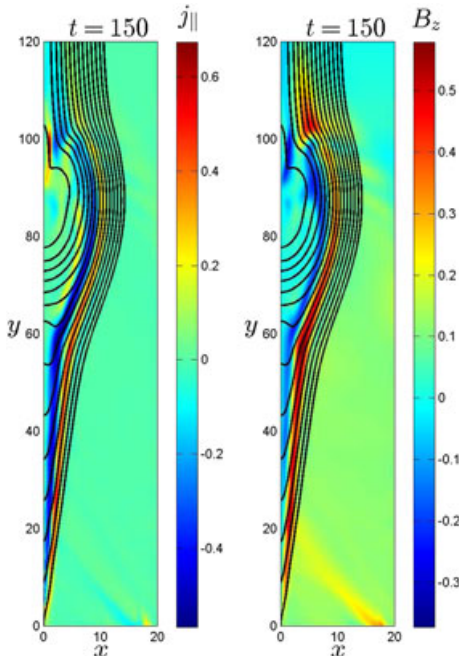

Figure 10. FAC density $j_\parallel$ and magnetic B_z component at $t = 150$ for Hall MHD reconnection case.
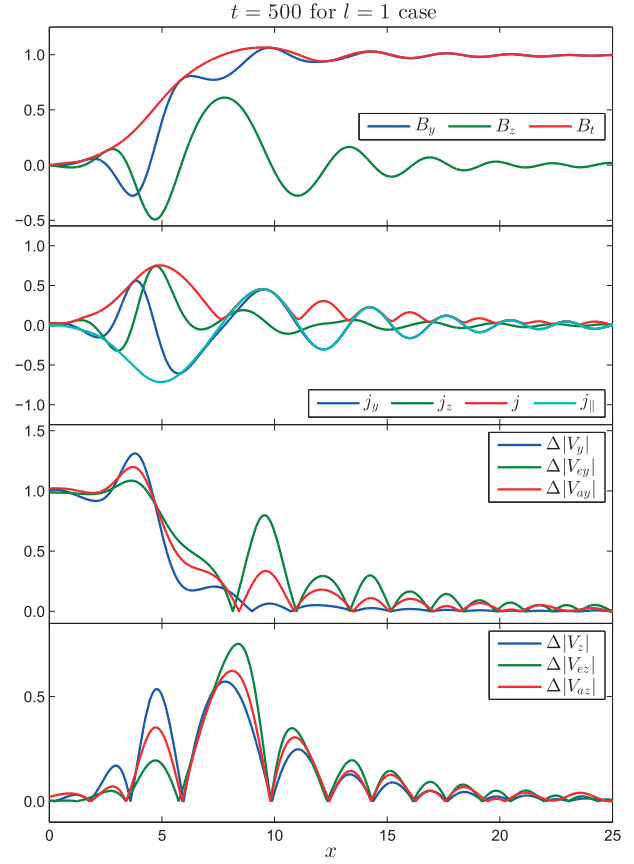

Figure 11. Profile of the reconnection layer at $t = 500$ for $l = 1$ and $p_\infty = 0.25$ case. The top panel shows B_y, B_z, and B_t; the middle panel shows j_y, j_z, j, and $j_\parallel$; and the bottom two panels shows ΔV_y, ΔV_{ey}, ΔV_{ay}, ΔV_z, ΔV_{ez}, and ΔV_{az} for walén test.

of $K_\parallel$ which is relevant for the ionospheric magnitude of the FAC. Although both cases, guide field and shear flow, generate significant FAC, the total current that can potentially be observed in the ionosphere is typically larger in the presence of shear flow.

3.3. Hall Physics Cases

[23] To conclude this examination of FAC generation, it is worth to consider the effects of Hall physics. Here the generation of FAC occurs without a guide field or shear flow for the bulk plasma. The magnetic field is frozen to the electron fluid, such that the motion by the electron current is sufficient to deflect the magnetic field into the invariant direction. Figure 10 shows magnetic field B_z component and the FAC density $j_\parallel$ at $t = 150$ for Hall MHD case ($B_{z0} = 0$, $V_{z0} = 0$, and $l = 1$). The bipolar structure of magnetic field B_z component extends all the way along the outflow region, instead of being localized in the vicinity of the reconnection region as observed by the Geospace Environment Modeling (GEM) challenge [*Otto*, 2001]. The FAC density $j_\parallel$ is located along the entire boundary of the outflow region and has the similar bipolar structure as B_z.

[24] Figure 11 shows the structure of the reconnection layer in Hall MHD case ($l = 1$), which demonstrates that the switch-off shock is replaced by a standing whistler wave,
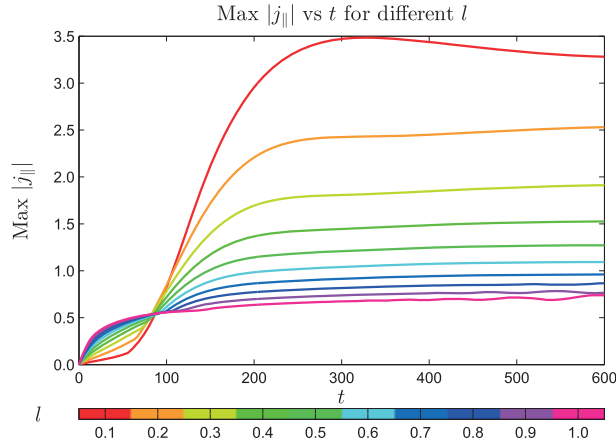
Figure 12. The evolution of max $j_\parallel$ in the reconnection layer for different l varying from 0.1 to 1.

Figure 14. The evolution of $I_\parallel$ in the reconnection layer for different Hall parameter l.

and the bipolar structure is a part of this wave. The physical explanation for this standing wave is as follows: the large-scale jump conditions imposed by MHD are the same for Hall MHD, and this solution requires a strong current in the z direction to turn off the magnetic field B_y component. In MHD, this is accomplished by slow switch-off shocks (in the symmetric case). However, in Hall MHD, a large current density in the z direction combined with the frozen-in condition for electrons implies a deflection of the magnetic field into the z direction. Apparently, this deflection is the source of a standing whistler wave downstream of the maximum current density. The middle panel of Figure 11 shows that the current density is much lower in Hall MHD than in MHD, because transition region depends on the wavelength of the whistle wave and becomes much wider. The magnitude of FAC density is almost identical to the total current density, which is similar to the RD. However, the direction of FAC density is alternating, contrary to a RD.

[25] It is well known that rotational discontinuities, intermediate shocks, and switch-off shocks satisfy the Walén relation $\Delta \mathbf{V} = \Delta \mathbf{V}_a = \Delta \left(\mathbf{B}/\sqrt{\rho} \right)$ for Alfvén waves. The bottom two panels of Figure 11 show the Alfvén velocity change $|\Delta \mathbf{V}_A|$, ion velocity change $|\Delta \mathbf{V}|$, and electron
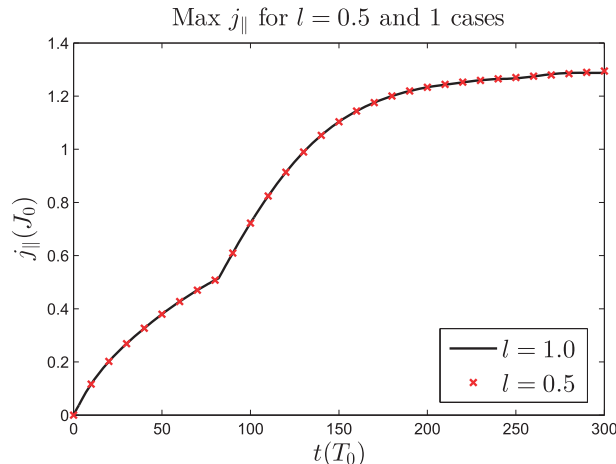
velocity change $|\Delta \mathbf{V}_e|$, which illustrates that in Hall MHD, both ions and electron also approximately satisfy the Walén relation. It is interesting that the small deviations between Alfvén speed variation and plasma bulk and electron velocity appear systematic up- and downstream of the outflow boundary. Such a systematic deviation has not yet been identified in observations, but it might be interesting to examine whether such a systematic deviation from the Alfvén speed is present for the plasma bulk and electron velocity. However, it is interesting to note that test of the Walén relation in observations often show deviations particularly for thin boundaries. It has been argued that such deviation may occur due to pressure anisotropy and which this is a possible cause, a Walén test on scales comparable to the ion inertia scale may reveal the modifications induced by the whistler dynamics.

[26] These extended standing waves are not visible in the two-dimensional Hall MHD results which show just the first maximum and minimum (bipolar B_z) of these waves due to a lack of resolution. The one-dimensional results use a resolution about 10 times better than in the two-dimensional simulation. It is not clear if this whistler wave can be observed by satellites, because the smaller amplitude waves can be concealed by the typical noise in space plasma and the waves could also be suppressed by ion gyroviscous effects.

[27] Figure 12 presents the evolution of the maximum FAC density magnitude max $|j_\parallel|$ in the reconnection layer for different Hall parameter l varying from 0.1 to 1 indicated by different colors, which shows that the max $|j_\parallel|$ decreases with increasing l. Naively, the opposite is expected, i.e., a decreasing max $|j_\parallel|$ with decreasing Hall parameter l, since there is no FAC for $l = 0$, as observed in the three-dimensional simulation results [*Ma and Lee*, 2001]. However, a rigorous examination shows that this is not correct for the following reason. The Hall MHD equations have no intrinsic scale except for the ion inertia scale λ_i. For example, a value of $l = 0.5$ implies the choice $L_0 = 2\lambda_i$. For a fixed ion inertia scale, the cases with $l = 1$ and $l = 0.5$ only imply a different normalization of the length scale L_0 for these cases. This can easily be removed by renormalizing the $l = 0.5$ case, as it is nicely shown in Figure 13. Here we have renormalized the $l = 0.5$ case with $L_0' = 0.5L_0$ which increases the normalization of current density by a factor of

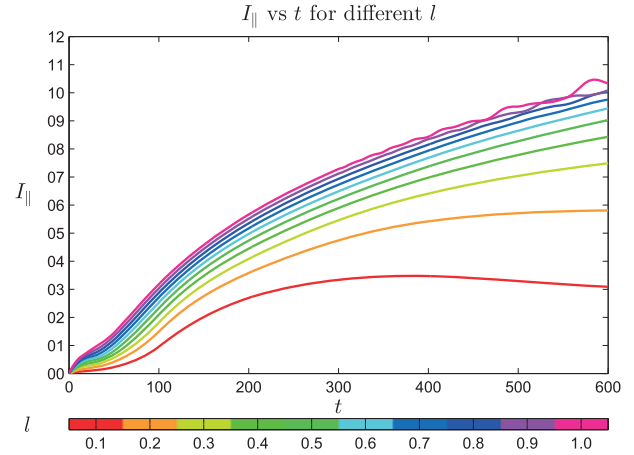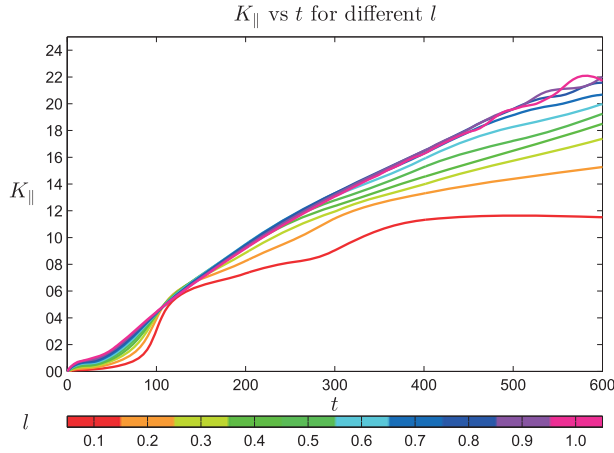**Figure 13.** The evolution of renormalized max $j_\parallel$ in the reconnection layer for $l = 0.5$ and 1 case.

Figure 15. The evolution of $K_{\parallel}$ in the reconnection layer for different Hall parameter l.

two, and therefore, leads to a current of half its value in normalized units. Note to compare the temporal evolution of the $l = 1$ and $l = 0.5$ cases, one would need to consider the renormalization of the time scale. This implies that the maximum current density should vary as l^{-1} for different values of l and time should be multiplied with l.

[28] At first glance, one might disagree with this argument because it leads to an infinite current density in the limit $l \rightarrow 0$. However, this arbitrarily large current is also concentrated in arbitrarily thin region. This is not possible in a numerical simulation with limitations on resolution and dissipation of structure below a resolution threshold. Therefore, the decrease of max $j_{\parallel}$ is an artifact of the limited resolution in a numerical simulation. Note that max $|j_{\parallel}|$ in the results presented here is much higher than in the three-dimensional studied by *Ma and Lee* [2001], because the resolution and resistivity in our study is better and specifically for values of $l = 1$ appropriate to address the ion inertia physics.

[29] Figures 14 and 15 show the evolution of $I_{\parallel}$ and $K_{\parallel}$ in the reconnection layer for different Hall parameter l, respectively. Note that the increase of $I_{\parallel}$ and $K_{\parallel}$ with increasing Hall parameter is opposite to the change of max $|j_{\parallel}|$. These integrals contain the product of length scale and current density, and this product is independent of a renormalization (the factors for length and current density cancel). However, a renormalization should be applied to the time scale. In other words, the time 600 for $l = 0.8$ corresponds to the time 300 for $l = 0.4$ and the deviation is mainly caused by the initial current width. Finally, it is noted that both $I_{\parallel}$ and $K_{\parallel}$ increase with time. This is likely caused by the expanding standing whistler wave structure at the outflow boundary which contributes additional FAC. In summary, two-dimensional magnetic reconnection, in the presence of Hall physics, leads to a strong generation of FAC, as long as the typical length scale is sufficiently resolved. In a real system, the Hall effect can be modified by gyro effects.

4. Summary and Discussion

[30] Satellite observations provide evidence for the generation of FAC during magnetic reconnection. To better understand the mechanisms of FAC formation in two-dimensional magnetic reconnection, three selected configurations have

been carefully studied. For reconnection with a guide field component, FACs are present already in the initial state, such that the FACs observed in magnetic reconnection are partly a projection and redistribution effect. However, guide field reconnection replaces the switch-off shocks of Petschek reconnection with a TDIS and a slow shock in the reconnection transition layer. All of FACs are generated in the TDIS layers. The slow shock layers are much thinner than the intermediate shock layers and ideally should satisfy the coplanarity condition such that the small associated FACs are either the result of a small deviation from the slow shock solution or a numerical artifact. For a small guide field component, a larger total FAC can be generated by reconnection because of the required larger magnetic field rotation. Vice versa, a large guide field implies less rotation of the magnetic field such that the projection effect is more important. Note that a large guide field component implies a smaller relative value of the antiparallel magnetic field components, such that magnetic reconnection is expected be slower on the Alfvén time scale based on the total magnetic field. The total amount of FAC $K_{\parallel}$ into the ionosphere is not sensitive to the initial (or asymptotic) guide field value.

[31] A perpendicular shear flow generates a B_z component and therefore FAC due to the frozen-in condition. The reconnection layer for a perpendicular shear flow configuration is similar to the reconnection layer in the guide field case. Since there is no FAC in the initial configuration, such currents are solely generated by the intermediate shock in the reconnection geometry. The total amount of FAC $K_{\parallel}$ is largely independent of the initial shear flow for values equal or larger than 0.2. The current into the ionosphere is generally larger for shear flow than for guide field states and is almost independent of the shear flow magnitude, provided there are no perpendicular currents to defect the FAC.

[32] The inclusion of Hall physics leads to the separation of ion and electron speed, and the frozen-in condition only applies to the electrons. The switch-off shock layer in MHD is replaced by a standing whistler wave in Hall MHD. The often found B_z bipolar structure (also for FAC) is the primary part of this standing wave, and this bipolar structure extends all the way along the outflow region, instead of being localized in the vicinity of the reconnection region. Compared with previous three-dimensional simulations results, our results show a much higher max $|j_{\parallel}|$ likely because of much better resolution. The maximum FAC density magnitude max $|j_{\parallel}|$ does not increase with increasing Hall parameter but decreases with $1/l$ for increasing Hall parameter l. For a fixed physical ion inertia scale λ_i, a larger Hall parameter l implies a smaller normalization scale L_0, which increases the normalized current density J_0 and such that any change in the maximum FAC is solely caused by the normalization rather than any physical change. For the same argument, although $I_{\parallel}$ and $K_{\parallel}$ appear proportional to the Hall parameter, it can also be taken out by a renormalization of time. Both ions and electrons approximately satisfy the Walén relation.

[33] Our study shows that significant FACs can be generated in magnetic reconnection in the presence of a guide field or of a perpendicular shear flow. Significant FAC is also generated in the outflow region of antiparallel reconnection on length scales close to the ion inertia scale. These FACs can propagate through Alfvén waves into the

ionosphere. It is well known that field-aligned electric fields are often associated with strong field-aligned currents, such that the newly forming FAC layers are a likely source for field-aligned particle acceleration and associated auroral signatures. Note that for guide field and perpendicular shear flow case, FACs are symmetric about the *y* axis. This indicates a layered structure of FACs and possibly also of respective auroral signatures in the ionosphere. However, FAC generated by shear flow case may be modulated by the Kelvin-Helmholtz (KH) waves, because this configuration is KH unstable in three dimensions if the guide field is not too strong. Hall physics is important only close to the boundary of the outflow region, and the standing whistler wave leads to a multiple FAC layers with alternating directions of the FAC.

[34] It is noted that this study is based on symmetric configurations, while the real magnetopause is asymmetric, i.e., different densities, magnetic field magnitudes, and shear flow on the two sides of the boundary. Magnetic reconnection can be suppressed by diamagnetic drifts for large plasma beta β in the presence of a guide field and strong magnetic field asymmetry [*Swisdak et al.*, 2003]. However, our result still applies, provided that magnetic reconnection operates, because the underlying physics is determined only by the outflow region and is independent of the processes in the diffusion region. Qualitatively, the conclusions concerning the evolution of the TDIS and more importantly on FAC generation by guide magnetic fields, velocity shear, and Hall physics are still applicable for asymmetry configurations. This study also provides guidance and reference for more specific studies on the effects of asymmetry for the evolution of FAC.

References

Birn, J. (1989), Three-dimensional equilibria for the extended magnetotail and the generation of field-aligned current sheets, *J. Geophys. Res.*, *94*, 252–260, doi:10.1029/JA094iA01p00252.

Birn, J., and M. Hesse (1991), The substorm current wedge and field-aligned currents in MHD simulations of magnetotail reconnection, *J. Geophys. Res.*, *96*, 1611–1618, doi:10.1029/90JA01762.

Cao, F., and J. R. Kan (1987), Finite-Larmor-radius effect on field-aligned currents in hydromagnetic waves, *J. Geophys. Res.*, *92*, 3397–3401, doi:10.1029/JA092iA04p03397.

Lee, E., K. W. Min, D.-Y. Lee, J. Seon, and K. J. Hwang (2002), Effect of B_y in three-dimensional reconnection at the dayside magnetopause, *Phys. Plasmas*, *9*, 5070–5078, doi:doi:10.1063/1.1519240.

Lin, Y. (2001), Global hybrid simulation of the dayside reconnection layer and associated field-aligned currents, *J. Geophys. Res.*, *106*, 25,451–25,466, doi:10.1029/2000JA000184.

Lin, Y., and L. C. Lee (1993), Structure of reconnection layers in the magnetosphere, *Space Sci. Rev.*, *65*, 59–179, doi:10.1007/BF00749762.

Lin, Y., and L. C. Lee (1999), Reconnection layers in two-dimensional magnetohydrodynamics and comparison with the one-dimensional Riemann problem, *Phys. Plasmas*, *6*, 3131–3146, doi:10.1063/1.873553.

Lin, Y., L. C. Lee, and C. F. Kennel (1992), The role of intermediate shocks in magnetic reconnection, *Geophys. Res. Lett.*, *19*, 229–232, doi:10.1029/91GL03008.

Ma, Z. W., and L. C. Lee (1999), A simulation study of generation of field-aligned currents and Alfvén waves by three-dimensional magnetic reconnection, *J. Geophys. Res.*, *104*, 10,177–10,190, doi:10.1029/1999JA900083.

Ma, Z. W., and L. C. Lee (2001), Hall effects on the generation of field-aligned currents in three-dimensional magnetic reconnection, *J. Geophys. Res.*, *106*, 25,951–25,960, doi:10.1029/2000JA000290.

Ma, Z. W., L. C. Lee, and A. Otto (1995), Generation of field-aligned currents and Alfvén waves by 3D magnetic reconnection, *Geophys. Res. Lett.*, *22*, 1737–1740, doi:10.1029/95GL01430.

Ogino, T. (1986), A three-dimensional MHD simulation of the interaction of the solar wind with the Earth's magnetosphere: The generation of field-aligned currents, *J. Geophys. Res.*, *91*, 6791–6806, doi:10.1029/JA091iA06p06791.

Otto, A. (1990), 3D resistive MHD computations of magnetospheric physics, *Comput. Phys. Commun.*, *59*, 185–195, doi:10.1016/0010-4655(90)90168-Z.

Otto, A. (2001), Geospace Environment Modeling (GEM) magnetic reconnection challenge: MHD and Hall MHD—constant and current dependent resistivity models, *J. Geophys. Res.*, *106*, 3751–3758, doi:10.1029/1999JA001005.

Otto, A., J. Büchner, and B. Nikutowski (2007), Force-free magnetic field extrapolation for MHD boundary conditions in simulations of the solar atmosphere, *Astron. Astrophys.*, *468*, 313–321, doi:10.1051/0004-6361:20054495.

Petschek, H. E. (1964), Magnetic Field Annihilation, in *The Physics of Solar Flares, Proceedings of the AAS-NASA Symposium held 28-30 October, 1963 at the Goddard Space Flight Center, Greenbelt, MD*, edited by W. N. Hess, p. 425, National Aeronautics and Space Administration, Science and Technical Information Division, Washington, D. C.

Sato, T., and T. Iijima (1979), Primary sources of large-scale Birkeland currents, *Space Sci. Rev.*, *24*, 347–366, doi:10.1007/BF00212423.

Sato, T., T. Hayashi, R. J. Walker, and M. Ashour-Abdalla (1983), Neutral sheet current interruption and field-aligned current generation by three-dimensional driven reconnection, *Geophys. Res. Lett.*, *10*, 221–224, doi:10.1029/GL010i003p00221.

Sato, T., R. J. Walker, and M. Ashour-Abdalla (1984), Driven magnetic reconnection in three dimensions: Energy conversion and field-aligned current generation, *J. Geophys. Res.*, *89*, 9761–9769, doi:10.1029/JA089iA11p09761.

Scholer, M., and A. Otto (1991), Magnetotail reconnection: Current diversion and field-aligned currents, *Geophys. Res. Lett.*, *18*, 733–736, doi:10.1029/91GL00361.

Song, Y., and R. L. Lysak (1994), Alfvénon, driven reconnection and the direct generation of the field-aligned current, *Geophys. Res. Lett.*, *21*, 1755–1758, doi:10.1029/94GL01327.

Sun, X., Y. Lin, and X. Wang (2005), Structure of reconnection layer with a shear flow perpendicular to the antiparallel magnetic field component, *Phys. Plasmas*, *12*, 012305, doi:10.1063/1.1826096.

Swisdak, M., B. N. Rogers, J. F. Drake, and M. A. Shay (2003), Diamagnetic suppression of component magnetic reconnection at the magnetopause, *J. Geophys. Res.*, *108*, 1218, doi:10.1029/2002JA009726.

Ugai, M. (1991), Computer simulations of field-aligned currents generated by fast magnetic reconnection in three dimensions, *J. Geophys. Res.*, *96*, 21,173–21,181, doi:10.1029/91JA01792.

Vasyliunas, V. M. (1984), Fundamentals of current description, in *Magnetospheric Currents, Geophys. Monogr. Ser.,* vol. 28, edited by T. A. Potemra, pp. 63–66, AGU, Washington, D. C. doi:10.1029/GM028p0063.

Walthour, D. W., B. U. O. Sonnerup, and C. T. Russell (1995), Observation of a slow-mode shock in the dayside magnetopause reconnection layer, *Adv. Space Res.*, *15*, 501–506, doi:10.1016/0273-1177(94)00135-N.

Wang, X. Y., C. S. Wu, S. Wang, J. K. Chao, Y. Lin, and P. H. Yoon (2001), A source of energetic particles associated with solar flares, *The Astrophys. J.*, *547*, 1159–1166, doi:10.1086/318395.